The Astrophysical Journal Letters, 896:L21 (8pp), 2020 June 20 https://doi.org/10.3847/2041-8213/ab9595

VLA–ALMA Spectroscopic Survey in the Hubble Ultra Deep Field (VLASPECS): Total Cold Gas Masses and CO Line Ratios for $z = 2$–3 Main-sequence Galaxies

Dominik A. Riechers[1,2], Leindert A. Boogaard[3], Roberto Decarli[4], Jorge González-López[5], Ian Smail[6], Fabian Walter[2,7], Manuel Aravena[8], Christopher L. Carilli[7,9], Paulo C. Cortes[10,11], Pierre Cox[12], Tanio Díaz-Santos[8,13,14], Jacqueline A. Hodge[3], Hanae Inami[15], Rob J. Ivison[16], Melanie Kaasinen[2,17], Jeff Wagg[18], Axel Weiß[19], and Paul van der Werf[3]

[1] Department of Astronomy, Cornell University, Space Sciences Building, Ithaca, NY 14853, USA; riechers@cornell.edu
[2] Max-Planck-Institut für Astronomie, Königstuhl 17, D-69117 Heidelberg, Germany
[3] Leiden Observatory, Leiden University, P.O. Box 9513, NL-2300 RA Leiden, The Netherlands
[4] INAF-Osservatorio di Astrofisica e Scienza dello Spazio, via Gobetti 93/3, I-40129 Bologna, Italy
[5] Carnegie Observatories, 813 Santa Barbara Street, Pasadena, CA 91101, USA
[6] Centre for Extragalactic Astronomy, Department of Physics, Durham University, South Road, Durham DH1 3LE, UK
[7] National Radio Astronomy Observatory, Pete V. Domenici Array Science Center, P.O. Box O, Socorro, NM 87801, USA
[8] Núcleo de Astronomía de la Facultad de Ingeniería y Ciencias, Universidad Diego Portales, Av. Ejército Libertador 441, Santiago, Chile
[9] Battcock Centre for Experimental Astrophysics, Cavendish Laboratory, Cambridge CB3 0HE, UK
[10] Joint ALMA Observatory—ESO, Av. Alonso de Córdova, 3104, Santiago, Chile
[11] National Radio Astronomy Observatory, 520 Edgemont Road, Charlottesville, VA 22903, USA
[12] Sorbonne Université, UPMC Université Paris 6 and CNRS, UMR 7095, Institut d'Astrophysique de Paris, 98bis boulevard Arago, F-75014 Paris, France
[13] Chinese Academy of Sciences South America Center for Astronomy (CASSACA), National Astronomical Observatories, CAS, Beijing 100101, People's Republic of China
[14] Institute of Astrophysics, Foundation for Research and Technology—Hellas (FORTH), Heraklion, GR-70013, Greece
[15] Hiroshima Astrophysical Science Center, Hiroshima University, 1-3-1 Kagamiyama, Higashi-Hiroshima, Hiroshima 739-8526, Japan
[16] European Southern Observatory, Karl-Schwarzschild-Straße 2, D-85748 Garching, Germany
[17] Universität Heidelberg, Zentrum für Astronomie, Institut für Theoretische Astrophysik, Albert-Ueberle-Straße 2, D-69120 Heidelberg, Germany
[18] SKA Organization, Lower Withington Macclesfield, Cheshire SK11 9DL, UK
[19] Max-Planck-Institut für Radioastronomie, Auf dem Hügel 69, D-53121 Bonn, Germany
Received 2020 April 24; revised 2020 May 18; accepted 2020 May 19; published 2020 June 15

Abstract

Using the NSF's Karl G. Jansky Very Large Array (VLA), we report six detections of CO($J = 1 \rightarrow 0$) emission and one upper limit in $z = 2$–3 galaxies originally detected in higher-J CO emission in the Atacama Large Millimeter/submillimeter Array Spectroscopic Survey in the Hubble Ultra Deep Field (ASPECS). From the CO($J = 1 \rightarrow 0$) line strengths, we measure total cold molecular gas masses of $M_{\rm gas} = (2.4\text{–}11.6) \times 10^{10}$ $(\alpha_{\rm CO}/3.6) M_{\odot}$. We also measure a median CO($J = 3 \rightarrow 2$) to CO($J = 1 \rightarrow 0$) line brightness temperature ratio of $r_{31} = 0.84 \pm 0.26$, and a CO($J = 7 \rightarrow 6$) to CO($J = 1 \rightarrow 0$) ratio range of $r_{71} < 0.05$ to $r_{71} = 0.17$. These results suggest that CO($J = 3 \rightarrow 2$) selected galaxies may have a higher CO line excitation on average than CO($J = 1 \rightarrow 0$) selected galaxies, based on the limited, currently available samples from the ASPECS and VLA CO Luminosity Density at High Redshift (COLDz) surveys. This implies that previous estimates of the cosmic density of cold gas in galaxies based on CO($J = 3 \rightarrow 2$) measurements should be revised down by a factor of $\simeq$2 on average based on assumptions regarding CO excitation alone. This correction further improves the agreement between the best currently existing constraints on the cold gas density evolution across cosmic history from line scan surveys, and the implied characteristic gas depletion times.

Unified Astronomy Thesaurus concepts: Galaxy evolution (594); Molecular gas (1073); Star formation (1569); Redshift surveys (1378); Galaxy formation (595); Observational astronomy (1145); Radio observatories (1350)

1. Introduction

Detailed studies of the star formation history of the universe, i.e., the volume density of star formation activity with redshift, have shown that, ~10 billion years ago, "typical" and starburst galaxies were forming 10–30 times more stars per year than at the present day. The observed buildup of stars is consistent with measurements of the volume density of stellar mass in galaxies through cosmic times (see, e.g., Madau & Dickinson 2014 for a review). Studies of the cold molecular gas, the prospective fuel for star formation, and gas mass fractions in high-redshift galaxies (see, e.g., Carilli & Walter 2013; Combes 2018 for reviews) suggest that this higher star formation activity is primarily due to an increased availability of fuel, rather than fundamental differences in the star formation process at earlier epochs (e.g., Daddi et al. 2010; Riechers et al. 2011c; Ivison et al. 2011; Bothwell et al. 2013; Tacconi et al. 2013, 2018; Genzel et al. 2015; Scoville et al. 2017; Kaasinen et al. 2019).

The rise of a new generation of powerful radio to sub/millimeter wavelength interferometers such as the NSF's Karl G. Jansky Very Large Array (VLA), the Atacama Large Millimeter/submillimeter Array (ALMA), and Northern Extended Millimeter Array (NOEMA) over the past decade is now enabling the first comprehensive view of the baryon cycle, i.e., the conversion from gas to stars over cosmic time, unveiling how galaxies grow across the history of the universe. This has only recently become possible based on the first large cosmic volume surveys for the cold gas density evolution at high redshift through the VLA CO Luminosity Density at High Redshift (COLDz; e.g., Pavesi et al. 2018; Riechers et al. 2019) and ALMA Spectroscopic Survey in the Hubble Ultra Deep Field (ASPECS; e.g., Walter et al. 2016; Decarli et al. 2019) CO line scan surveys. Together with an earlier

pilot study with PdBI/NOEMA in the Hubble Deep Field (Decarli et al. 2014; Walter et al. 2014), these surveys have now covered a volume approaching 500,000 Mpc^3. In the most sensitive areas, these studies reach down to galaxies below the characteristic CO luminosity L'_{CO} out to at least $z \sim 3$, showing that they select representative star-forming galaxies at high redshift. Despite the fact that they cover different survey fields, the cosmic gas density measurements of ASPECS and COLDz are remarkably consistent, showing that cosmic variance likely is not the dominant source of uncertainty of the measurements at this stage (see also Popping et al. 2019). However, one remaining source of uncertainty is due to the fact that these surveys cover different CO transitions in the overlapping redshift ranges. In particular, COLDz measures CO($J = 1 \rightarrow 0$) emission at $z = 2$–3, while ASPECS measures CO($J = 3 \rightarrow 2$) emission at the same redshift. To address possible uncertainties due to CO excitation, the ASPECS measurements are "corrected" by adopting a CO($J = 3 \rightarrow 2$) to CO($J = 1 \rightarrow 0$) line brightness temperature ratio of $r_{31} = 0.42 \pm 0.07$, based on previous measurements of three main-sequence galaxies at $z \simeq 1.5$ (i.e., the closest comparison sample available at the time; Daddi et al. 2015) before adopting an α_{CO} conversion factor to translate the inferred CO($J = 1 \rightarrow 0$) line luminosities to gas masses (see Decarli et al. 2019 for details).

We here present VLA observations of the Hubble Ultra Deep Field (HUDF) in a region covered by ASPECS at higher frequencies (i.e., in higher-J CO lines) to derive more robust estimates of CO line brightness temperature ratios for gas-selected galaxies by constraining the gas excitation in the low-J CO lines. We use these data to measure total cold molecular gas masses, gas depletion times, and baryonic gas mass fractions. Our observations cover seven of the eight ASPECS sources in the $z = 2$–3 redshift range, and thus provide direct measurements of most of the sources that are used to infer the cosmic gas density measurements near the peak of the cosmic star formation history in this field. We describe the observations in Section 2, and present the results in Section 3. Further analysis and a discussion of the impact of our findings are given in Section 4, before we provide a summary and conclusions in Section 5. We use a concordance, flat Λ CDM cosmology throughout, with $H_0 = 69.6\ \mathrm{km\,s^{-1}\,Mpc^{-1}}$, $\Omega_{\mathrm{M}} = 0.286$, and $\Omega_{\Lambda} = 0.714$ (Bennett et al. 2014).

2. Data

We used the VLA to observe redshifted CO($J = 1 \rightarrow 0$) emission (rest-frame frequency: $\nu_{\mathrm{rest}} = 115.2712$ GHz) in seven galaxies in the HUDF at $z = 2.0$–2.7 (VLA program ID: 19B-131; PI: Riechers). We used the *Ka*-band receivers in combination with the WIDAR correlator configured to 3-bit sampling mode to observe a contiguous bandwidth of 8 GHz (dual polarization) covering the 30.593–38.662 GHz (i.e., ∼9 mm) frequency range at 2 MHz spectral resolution (17 $\mathrm{km\,s^{-1}}$ at 35 GHz). Some minor overlaps between subbands were employed to avoid that the centers of known lines fall onto subband gaps. Gaps between subbands were mitigated by employing three frequency switching setups, shifted by ±12 MHz relative to the central setup. To cover all targets, as well as ∼120 fainter galaxies with secure optical spectroscopic redshifts for which the CO($J = 1 \rightarrow 0$) or CO($J = 2 \rightarrow 1$) line is accessible within our data set, two telescope pointings centered at (J2000 03:32:43.294, −27:46:44.88) and (03:32:38.834, −27:46:35.46) were observed to equal depth. Observations were carried out under very good weather conditions in D array using 17 scheduling blocks with a length of 2.5 hr each between 2019 December 7 and 2020 January 27. This resulted in a total time of 42.5 hr, or 14.7 hr on source per pointing.[20] Given the decl. of the HUDF, 4 of the 27 antennas were shadowed by other antennas and thus flagged in all data sets. The radio quasar J0348−2749 ($S_\nu = 1.79 \pm 0.13$ Jy based on our calibration, which provides individual values covering the 1.61–1.99 Jy range) was observed every 9 minutes for complex gain calibration. The quasar 3C 48 ($S_\nu = 0.70$–0.88 Jy from the upper to the lower frequency edges of the bandpass, based on the Perley & Butler 2017 scale) was observed once per scheduling block for flux calibration. Given its recent flaring activity,[21] we conservatively consider the absolute flux calibration to be reliable at the ∼15% uncertainty level.

All data were processed with the CASA 5.6.2 pipeline, augmented by manual data editing where necessary. Imaging the data in mosaicking mode with natural baseline weighting out to the 10% primary beam response[22] region yields a synthesized clean beam size of $4\farcs99 \times 1\farcs96$ (largest recoverable scale: ∼45″) and an rms noise level of 1.8 μJy $\mathrm{beam^{-1}}$ across the entire 8 GHz continuum bandwidth covered by the spectral setup. The noise level increases by nearly a factor of 2 from the low- to the high-frequency edge of the bandpass, as expected based on the increasing receiver and atmospheric noise temperatures with frequency in the *Ka* band. The rms noise in the phase centers is 40–44 μJy $\mathrm{beam^{-1}}$ per 75 $\mathrm{km\,s^{-1}}$ bin at the line frequencies of all targets except the lowest-redshift source, where it is 70 μJy $\mathrm{beam^{-1}}$.

3. Results

We robustly detected CO($J = 1 \rightarrow 0$) emission toward three targets at $>4.5\sigma$ significance and tentatively detect another three at ∼2.5–4.0σ, but we have not detected the seventh target (which lies in a region where sensitivity is reduced by a factor of ∼3.5 due to primary beam attenuation). We extracted spectra at the map peak positions of all targets from the primary beam corrected mosaic (or from the ALMA CO $J = 3 \rightarrow 2$ peak position for the nondetection), and fitted them with Gaussian line profiles (Figure 1 and the Appendix). We then created moment-0 maps across the velocity ranges where emission is seen in the spectra. ASPECS-LP.9mm.1, 2, 3, 4, 5, and 6 (hereafter: 9mm.1 to 6) are detected at peak signal-to-noise ratios of 6.2, 6.4, 4.8, 4.0, 3.6, and 2.5, respectively, in the moment-0 maps (Figure 1). We then fitted two-dimensional Gaussian profiles in the image plane to the emission in the moment-0 maps to investigate if sources are extended.[23] All sources except 9mm.1 and 3 are consistent with point sources. 9mm.1 has a formal deconvolved size of $(4.7 \pm 2.4) \times (1.1 \pm 0.7)\ \mathrm{arcsec^2}$, which corresponds to $(39 \pm 19) \times (9 \pm 6)\ \mathrm{kpc^2}$. 9mm.3 has a formal deconvolved size of $(4.7 \pm 2.0) \times (1.0 \pm 1.6)\ \mathrm{arcsec^2}$, which corresponds to $(38 \pm 16) \times (8 \pm 13)\ \mathrm{kpc^2}$.[24] Both sources are smaller than the beam, and thus are marginally resolved along their source major axes (which are close to the VLA beam minor axes) at best. The extension of

[20] A total of 82.5 hr were approved, but could not be completed due to weather and scheduling constraints given the low decl. of the HUDF.

[21] See https://science.nrao.edu/facilities/vla/docs/manuals/oss/performance/fdscale, version 2019 November 19.

[22] The VLA primary beam full-width at half-power at our observing frequencies is ∼65″–82″.

[23] Uncertainties from these fits are propagated to the reported line fluxes.

[24] 9mm.5 is best fitted with a finite size, resulting in a formal deconvolved size of $(1.7 \pm 1.8) \times (0.4 \pm 1.5)\ \mathrm{arcsec^2}$, which corresponds to $(14 \pm 15) \times (3 \pm 13)\ \mathrm{kpc^2}$. Given that the source is only tentatively detected and the resulting significant uncertainties, we only consider this a weak constraint.

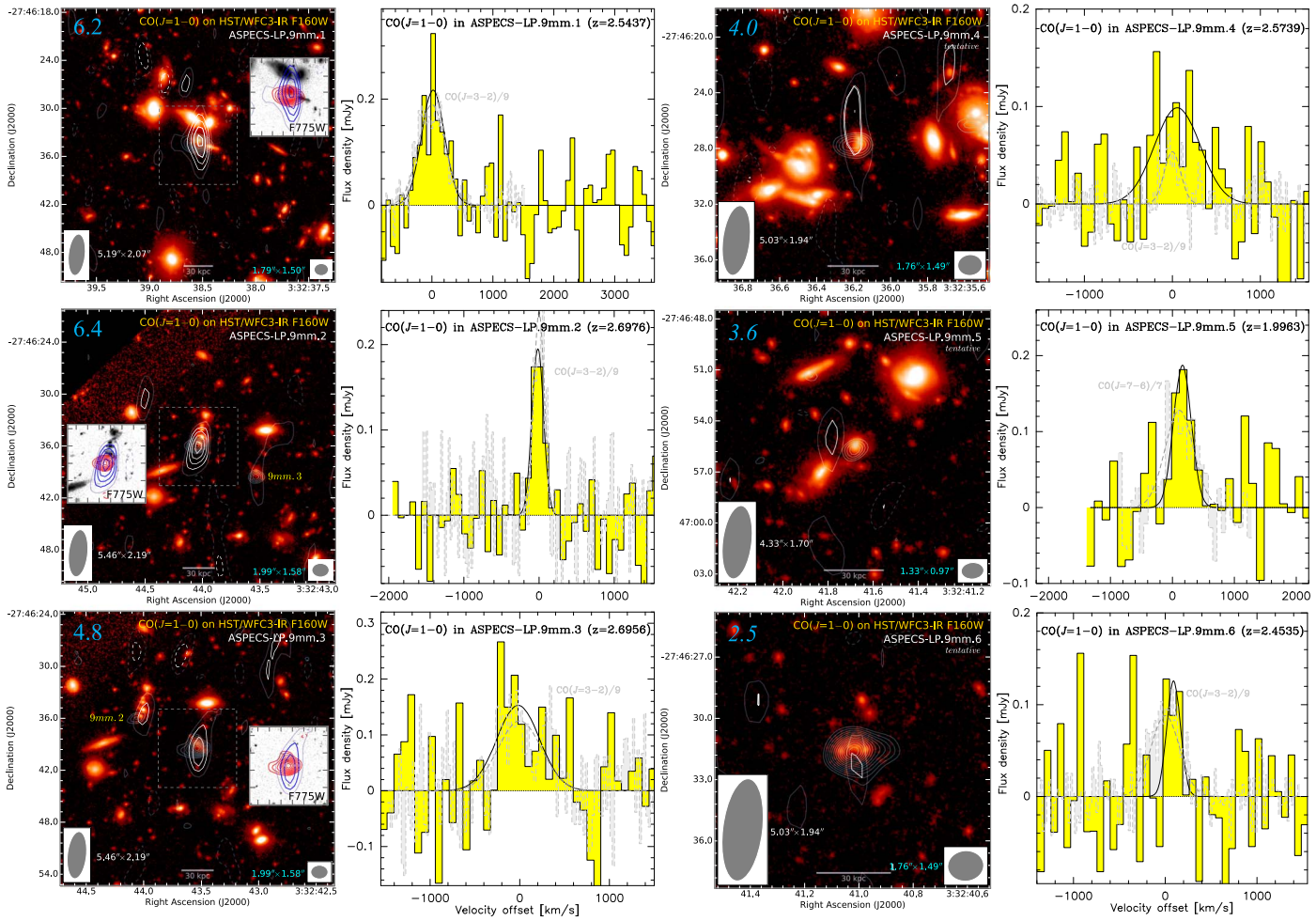

Figure 1. VLA CO($J = 1 \rightarrow 0$) moment-0 line maps (left panels; white contours) and line spectra (right panels; solid histograms) of all detected galaxies in the sample, and Gaussian fits to the line profiles (black curves) where applicable. Contour maps are shown overlaid on HST/WFC3-IR F160W images, and ACS F775W insets for the robust detections (Illingworth et al. 2013), with CO($J = 1 \rightarrow 0$) peak signal-to-noise ratios indicated in blue in the top left corner of each map panel. ALMA CO($J = 3 \rightarrow 2$) or CO($J = 7 \rightarrow 6$) (9mm.5 only) contours from González-López et al. (2019) or B20 are shown for comparison (aqua color). VLA maps are integrated over 737, 192, 923, 632, 405, and 341 km s^{-1} (80, 20, 96, 68, 52, and 38 MHz), for 9mm.1, 2, 3, 4, 5, and 6, respectively. VLA contour levels are in steps of $1\sigma = 14$, 25, 12.5, 14, 30, and 20.2 μJy beam^{-1}, starting at $\pm 2\sigma$ (except 9mm.6, where an additional 2.5σ contour level is shown). ALMA contour levels are in steps of $1\sigma = 27$, 65, 38, 37, 105, and 29 μJy beam^{-1}, starting at $\pm 3\sigma$, except 9mm.1, where contour steps are $\pm 3\sigma$. The VLA (ALMA) beam sizes are shown in the bottom left (right) corner of each panel. 9mm.5 shows an offset between the peak position of both lines, likely primarily due to the modest signal-to-noise ratio of the tentative CO($J = 1 \rightarrow 0$) detection. Spectra are shown at resolutions of 74, 77, 77, 74, 149, and 72 km s^{-1} (8, 8, 8, 8, 16, and 8 MHz), respectively. Velocity scales are relative to the redshifts indicated. Scaled ALMA CO($J = 3 \rightarrow 2$) or CO($J = 7 \rightarrow 6$) spectra (dashed gray histograms; González-López et al. 2019; B20) are shown for comparison.

9mm.1 appears to be consistent with that seen in the ALMA CO($J = 3 \rightarrow 2$) data (Figure 1). Future observations at higher resolution and greater sensitivity are necessary to better constrain the true sizes of these galaxies.

All line fluxes and widths and the corresponding line luminosities are summarized in Table 1. The line widths agree with those measured from the higher-J lines observed by ALMA within the uncertainties, with two exceptions. The tentatively detected CO($J = 1 \rightarrow 0$) line in 9mm.6 is narrower than the CO($J = 3 \rightarrow 2$) line by a factor of 2.1 ± 1.4. Upon inspection of the line profile, it becomes clear that the limited signal-to-noise ratio of the measurement did not allow for a detection of the faint blue line component seen by ALMA (which also causes a small offset in the peak velocities), such that the CO($J = 1 \rightarrow 0$) line width may be biased low because the Gaussian fit does not account for this component. On the other hand, the tentatively detected CO($J = 1 \rightarrow 0$) line in 9mm.4 is 2.8 ± 1.4 times broader than its CO($J = 3 \rightarrow 2$) line. Although the uncertainties are still significant, this may indicate the presence of an extended cold gas reservoir with low gas excitation, which could be partially missed in the higher-J CO line measurements. No higher-J lines than CO($J = 3 \rightarrow 2$) are detected in this source by ALMA (see L. Boogaard et al. 2020, in preparation, hereafter B20, for further details). However, this finding needs to be investigated further with more sensitive data. 9mm.5 may show slight differences in the line profiles between CO($J = 1 \rightarrow 0$) and CO($J = 7 \rightarrow 6$), which is consistent with a minor difference in peak velocities. If confirmed, this could be due to differential gas excitation across the galaxy, but no firm conclusions are possible at the current signal-to-noise ratio of the data (which likely is also responsible for the apparent spatial offset between the emission peaks). In all other cases, the peak position of the CO($J = 1 \rightarrow 0$) emission coincides with that of the higher-J CO emission and the stellar light within the uncertainties (Figure 1).

We convert the CO($J = 1 \rightarrow 0$) line luminosities to total cold molecular gas masses by adopting a conversion factor of

Table 1
VLASPECS Line Parameters

VLA ID	ALMA ID	$z_{\rm ALMA}$	$I_{\rm CO(1-0)}$ (Jy km s^{-1})	$dv_{\rm CO(1-0)}$ (km s^{-1})	$dv_{\rm ALMA}$[a] (km s^{-1})	$L'_{\rm CO(1-0)}$ (10^{10} K km s^{-1} pc^2)	$M_{\rm gas}$ ($10^{11} M_\odot$)	$f_{\rm gas}$[b]	$f_{\rm bary}$[c]	$t_{\rm dep}$[d] (Gyr)	r_{31}	r_{71}
9mm.1	3mm.1	2.5437	0.103 ± 0.022	447 ± 110	519 ± 18	3.22 ± 0.68	1.16 ± 0.24	4.6	0.82	0.46	0.84 ± 0.18	0.17 ± 0.05
9mm.2	3mm.9	2.6976	0.038 ± 0.006	201 ± 47	166 ± 24	1.32 ± 0.19	0.48 ± 0.07	0.38	0.27	0.15	1.10 ± 0.21	<0.93
9mm.3	3mm.7	2.6956	0.091 ± 0.022	560 ± 230	570 ± 70	3.14 ± 0.75	1.13 ± 0.27	0.90	0.47	0.57	0.79 ± 0.21	<0.21
9mm.4[e]	3mm.12	2.5739	*0.064 ± 0.019*	*620 ± 280*	221 ± 40	*2.03 ± 0.60*	*0.73 ± 0.22*	*1.84*	*0.65*	*2.3*	*0.23 ± 0.08*	*<0.05*
9mm.5[e]	1mm.C14a	1.9963	*0.065 ± 0.018*	*342 ± 96*	281 ± 57	*1.31 ± 0.37*	*0.47 ± 0.13*	*0.75*	*0.43*	*0.94*	⋯	*0.12 ± 0.04*
9mm.6[e]	3mm.3	2.4535	*0.022 ± 0.009*	*176 ± 110*	367 ± 31	*0.66 ± 0.26*	*0.24 ± 0.09*	*0.47*	*0.32*	*0.37*	*1.54 ± 0.61*	*<0.25*
9mm.7	1mm.C07	2.5805	<0.105 (3σ)	⋯	660 ± 110	<3.4	<1.2	<1.2	<0.55	<3.0	>0.17	>0.09

Notes. Stellar masses, star formation rates, and $J_{\rm upper} \geqslant 3$ CO line parameters used in the calculations were adopted from González-López et al. (2019) and B20 (see also Aravena et al. 2019; M. Aravena et al. 2020, in preparation). VLA primary beam correction factors of pbc = 0.984, 0.913, 0.970, 0.565, 0.785, 0.894, and 0.286 were adopted throughout for 9mm.1, 2, 3, 4, 5, 6, and 7, respectively. We here report CO($J = 1 \rightarrow 0$) line parameters based on a signal-to-noise ratio optimized extraction, i.e., without tying them to the ALMA measurements. Fixing the extraction to the ALMA-based line centroids and widths would yield changes in r_{31} by 6.4%, −11%, 0.6%, −57%, and 3.6% for 9mm.1, 2, 3, 4, and 6, respectively, or −0.08% on average when excluding 9mm.4. These differences are negligible compared to other sources of uncertainty for all sources except 9mm.4. Where not provided, we assume uncertainties of 25% for robustly CO($J = 1 \rightarrow 0$)-detected sources, and 40% for tentatively detected sources. r_{31} and r_{71} are CO($J = 3 \rightarrow 2$) to CO($J = 1 \rightarrow 0$) and CO($J = 7 \rightarrow 6$) to CO($J = 1 \rightarrow 0$) line brightness temperature ratios, respectively.

[a] Obtained from a simultaneous fit of all ALMA-detected CO/[C I] lines considered by B20, i.e., excluding the VLA CO($J = 1 \rightarrow 0$) measurements reported here.

[b] Defined as $f_{\rm gas} = M_{\rm gas}/M_\star$; also commonly referred to as the gas-to-stellar mass ratio $\mu_{\rm mol}$ or $\mu_{\rm gas}$ in the literature.

[c] Defined as $f_{\rm bary} = M_{\rm gas}/(M_{\rm gas} + M_\star)$.

[d] Defined as $t_{\rm dep} = M_{\rm gas}/{\rm SFR}$.

[e] Tentative detection; independent confirmation of line parameters from more sensitive data required.

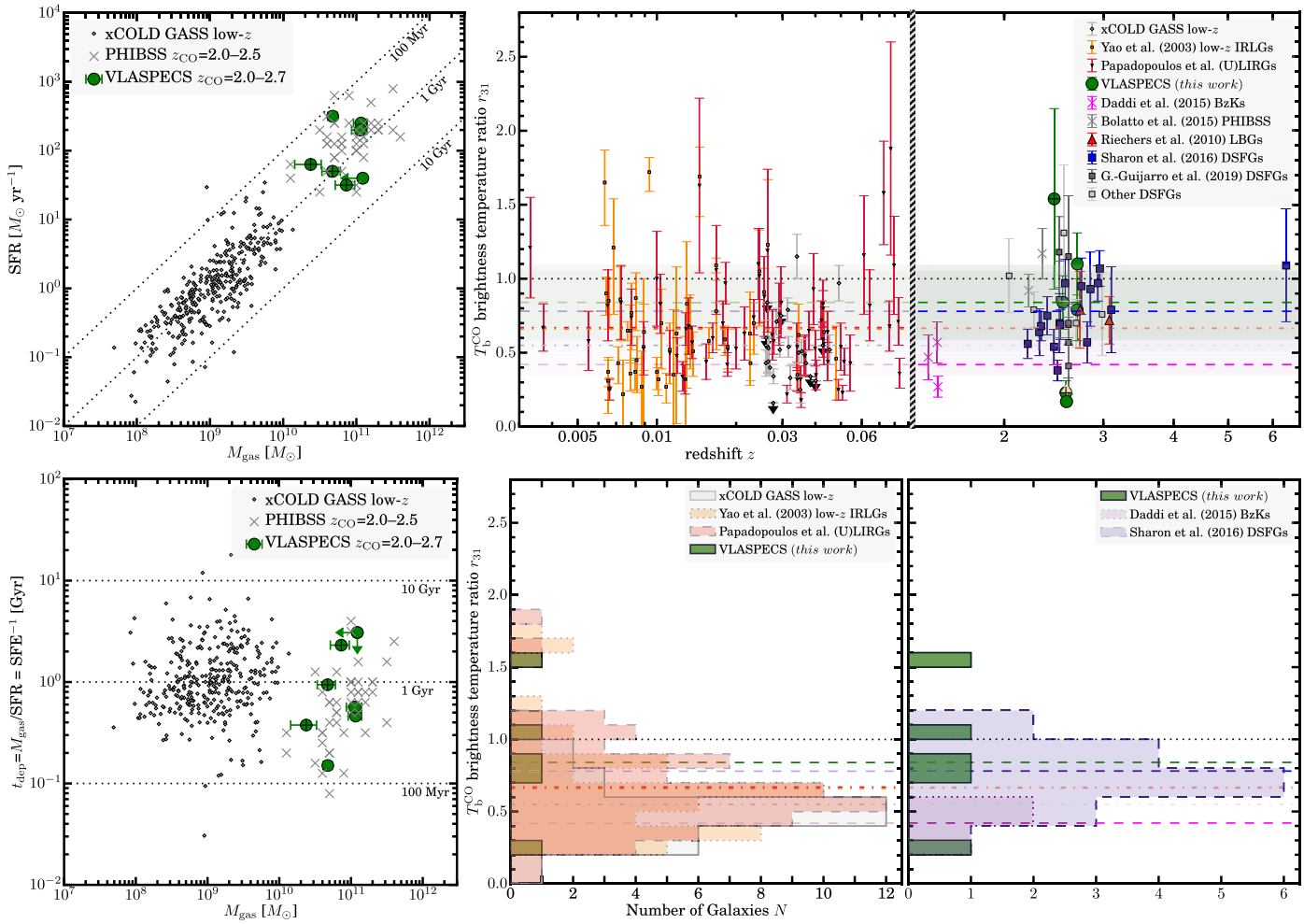

Figure 2. Top left: the revised, CO($J = 1 \rightarrow 0$)-based $M_{\rm gas}$ from VLASPECS confirm that $z = 2$–3 galaxies detected in the ASPECS survey (green circles; tentative detections are marked with a plus sign) closely follow the "star formation law" (i.e., $M_{\rm gas}$–SFR relation) at high redshift. CO-detected main-sequence galaxies at similar redshifts from the PHIBBS1/2 surveys (typically based on CO $J = 3 \rightarrow 2$, but using a metallicity-dependent conversion factor; Tacconi et al. 2018) and local galaxies from the xCOLD GASS CO($J = 1 \rightarrow 0$) survey (Saintonge et al. 2017) are shown for comparison. Bottom left: same as the top left panel, but plotting the depletion time $t_{\rm dep}$ against $M_{\rm gas}$. All samples cover a similar range in $t_{\rm dep}$, but the average $t_{\rm dep}$ for the (higher $M_{\rm gas}$) high-z samples appear lower. Top right: the r_{31} brightness temperature ratio of VLASPECS galaxies (green circles) is similar to that of strongly lensed $z \sim 3$ Lyman-break galaxies (red triangles; Riechers et al. 2010), $z > 2$ main-sequence galaxies from the PHIBSS survey (gray crosses; Bolatto et al. 2015), and $z > 2$ dusty star-forming galaxies (DSFGs; blue squares; compilation from Sharon et al. 2016; including data from Danielson et al. 2011; Ivison et al. 2011; Riechers et al. 2011a, 2011b, 2013; Thomson et al. 2012; Fu et al. 2013; Sharon et al. 2013, 2015; other DSFGs shown as light gray squares are from Nayyeri et al. 2017; Dannerbauer et al. 2019; Harrington et al. 2019; Leung et al. 2019; Sharon et al. 2019) and clustered DSFGs (dark gray squares; Bussmann et al. 2015; Gómez-Guijarro et al. 2019), but ~2 times higher on average than BzK-selected main-sequence galaxies at $z \sim 1.5$ (magenta crosses; Daddi et al. 2015). Nearby galaxy samples from the xCOLD GASS survey (Lamperti et al. 2020) and two studies of infrared-luminous galaxies (Yao et al. 2003; Papadopoulos et al. 2012) are shown for comparison. Dashed lines and shaded regions indicate mean/median values and spread for high-z samples with >2 galaxies or clusters, with the same color coding as the symbols. Dashed–dotted lines indicate mean values for the low-z samples. Bottom right: same as the top right panel, but shown as binned histograms in r_{31} (excluding upper limits) and across the full redshift range, and only including samples for which mean/median values are indicated in the top right panels.

$\alpha_{\rm CO} = 3.6\,M_\odot({\rm K\ km\,s^{-1}\,pc^2})^{-1}$, as was done in our previous work (e.g., Riechers et al. 2019; Decarli et al. 2019; see also Daddi et al. 2010), consistent with the stellar mass–metallicity relation (Boogaard et al. 2019; see also Aravena et al. 2019).[25] We also measure line brightness temperature ratios relative to the CO($J = 3 \rightarrow 2$) and CO($J = 7 \rightarrow 6$) lines, using the line fluxes measured from the ALMA data (B20, and references therein).

4. Analysis and Discussion

4.1. Gas Masses, Depletion Times, and Line Ratios

We find total cold molecular gas masses of (4.8–11.6) × $10^{10}\,M_\odot$ for our sample ((2.4–11.6) × $10^{10}\,M_\odot$ when including tentative detections), which corresponds to baryonic gas mass fractions of 27%–82%, and gas depletion times of 150–570 Myr (150 Myr–2.3 Gyr when including tentative detections; see Table 1). These galaxies thus follow the "star formation law" (i.e., $M_{\rm gas}$–SFR relation) for main-sequence galaxies at high redshift (Figure 2 (left)). Only 9mm.2 shows a short gas depletion time, as is characteristic of starburst galaxies.[26]

[25] Since the calibration of $\alpha_{\rm CO}$ depends on the ratio of the gas density n and the CO line brightness temperature $T_{\rm b}$ ($\alpha_{\rm CO} \propto \sqrt{n}\ T_{\rm b}^{-1}$ in the simplest case; e.g., Solomon & Vanden Bout 2005; Bolatto et al. 2013), it is expected to scale with CO excitation in practice. Our current constraints for the ASPECS sample appear to disfavor significantly lower $\alpha_{\rm CO}$ values than adopted in this work, but dynamical mass measurements from higher-resolution CO observations in the future will be required to more directly calibrate $\alpha_{\rm CO}$.

[26] Gas depletion times depend on the conversion factor, and would be shorter for lower $\alpha_{\rm CO}$ in principle.

We measure CO line brightness temperature ratios between the CO($J = 3 \rightarrow 2$) and CO($J = 1 \rightarrow 0$) lines of $r_{31} = 0.79$–1.10 for the robust line detections, or 0.23–1.54 when including tentative detections, with a median value of 0.84 ± 0.05 or 0.84 ± 0.26 and a mean value of 0.91 ± 0.14 or 0.90 ± 0.43 when excluding or including tentative detections, respectively.[27] This is comparable to the mean line ratios found for strongly lensed Lyman-break galaxies (Figure 2 (right); ∼0.75; Riechers et al. 2010) and dusty star-forming galaxies at similar redshifts (0.78 ± 0.27; Sharon et al. 2016; see also, e.g., Riechers et al. 2011a, 2011b; Ivison et al. 2011; Danielson et al. 2011; Thomson et al. 2012; Frayer et al. 2018), but twice as high as the value of $r_{31} = 0.42 \pm 0.07$ adopted in previous works (based on a sample of three $z \sim 1.5$ main-sequence galaxies from Daddi et al. 2015), suggesting that the gas masses at $z \sim 2.5$ estimated based on the ALMA measurements of the CO($J = 3 \rightarrow 2$) line alone should be corrected down by a factor of $\simeq$2 on average.

We also find line brightness temperature ratios between the CO($J = 7 \rightarrow 6$) and CO($J = 1 \rightarrow 0$) lines of $r_{71} < 0.05$–0.17, with additional, less constraining upper limits in the <0.21 to <0.93 range. The only robust detection in both lines is 9mm.1, with $r_{71} = 0.17 \pm 0.05$. Our findings suggest that, in lieu of observational constraints, $r_{71} = 0.1$–0.2 may be considered a reasonable assumption for $z = 2$–3 main-sequence galaxies, but we caution that 9mm.1 contains an active galactic nucleus (AGN).[28] This is comparable to the characteristic value proposed for dusty star-forming galaxies at similar redshifts ($r_{71} = 0.18 \pm 0.04$; Bothwell et al. 2013). It is also comparable to the mean value found for a sample of nearby luminous and ultraluminous infrared galaxies studied by Rosenberg et al. (2015), i.e., $r_{71} = 0.15 \pm 0.10$, but below the most highly excited sources in that sample (their "Class III" objects), $r_{71} = 0.24 \pm 0.11$. The latter subsample includes those galaxies for which an AGN contribution to the line excitation is the most plausible (such as Mrk 231; e.g., van der Werf et al. 2010), but it should be noted that current evidence indicating that AGN lead to changes in r_{71} remains ambiguous at best.[29] As an example, in the CO line excitation model for Mrk 231 shown by van der Werf et al. (2010), the starburst contribution to the CO($J = 7 \rightarrow 6$) flux is about three times higher than that by the AGN. Moreover, Lu et al. (2017) have suggested that the CO excitation ladder of Mrk 231 only significantly deviates from those of nearby starbursts like Arp 220 and M82 in the CO($J = 10 \rightarrow 9$) line and above.

4.2. Implications for the Cold Gas Density Evolution

Based on the ASPECS 3 mm data and adopting $r_{31} = 0.42 \pm 0.07$, Decarli et al. (2019) found a comoving cosmic molecular gas density of $\log(\rho(\mathrm{H_2})/M_\odot\,\mathrm{Mpc^{-3}}) = 7.26$–$8.10$ (2σ) in the HUDF for the $z = 2.0$–3.1 redshift range. Adopting our median $r_{31} = 0.84 \pm 0.26$ at face value as the best estimate would reduce this measurement to $\log(\rho(\mathrm{H_2})/M_\odot\,\mathrm{Mpc^{-3}}) = 6.96$–$7.80$ (2σ),[30] with an average of 7.44. In comparison, results from the COLDz survey in the COSMOS and GOODS-North fields at $z = 2.0$–2.8 (Riechers et al. 2019; see Figure 3) suggest $\log(\rho(\mathrm{H_2})/M_\odot\,\mathrm{Mpc^{-3}}) = 7.04$–$7.75$ (90% confidence boundary),[31] with an average of 7.43.[32] Thus, the constraints from both surveys in this redshift bin are indistinguishable when adopting our new constraints on r_{31}.

The ASPECS constraints in the $z = 0.3$–0.6 redshift interval are also based on CO($J = 3 \rightarrow 2$) measurements, whereas those at $z = 0.7$–1.2, and 3.0–4.5 are based on CO($J = 4 \rightarrow 3$) measurements, and they are scaled to line ratios for the same reference sample as the $z = 2.0$–3.1 bin (see Decarli et al. 2019). Our new measurements suggest that significant corrections may also be required for those measurements. The remaining bins are based on CO($J = 1 \rightarrow 0$) and CO($J = 2 \rightarrow 1$) measurements. Thus, the lowest-redshift bin at $z = 0.0$–0.4 is likely not affected by our new findings, while we estimate that the $z = 1.0$–1.7 bin is potentially affected at the $\lesssim$10%–20% level. If confirmed, this would suggest a lower redshift for the peak in the comoving gas density than previously assumed.[33] In light of these findings, an upcoming publication will quantitatively address the required changes based on the full CO excitation ladders of all ASPECS galaxies in more detail (B20), to fully assess the consequences of our new findings on the cold gas density history of the universe.

5. Summary and Conclusions

Using the VLA, we have measured CO($J = 1 \rightarrow 0$)-based gas masses, gas depletion times, and baryonic gas fractions for six galaxies discovered by the ASPECS survey in the HUDF, and we obtained an upper limit for a seventh source.[34] This independently confirms that these galaxies are gas-rich, and in some cases, gas-dominated massive galaxies that are representative of the "typical" galaxy population at $z = 2$–3 in terms of their star formation rates (SFRs) and stellar masses. Based on these measurements, we revise previous estimates of the gas masses in this redshift bin down by a factor of 2 on average. These findings improve the agreement between measurements of the cold gas mass density evolution with redshift from the ASPECS and COLDz surveys, further demonstrating the reliability of the constraints obtained from millimeter-wave line scan surveys across large cosmic volumes. Comparing the ASPECS and COLDz samples (D. Riechers et al. 2020, in preparation), there may be a hint that CO($J = 3 \rightarrow 2$) selected galaxies could have higher CO line excitation on average than CO($J = 1 \rightarrow 0$) selected galaxies, but current sample sizes are too small to provide a firm conclusion.

The ASPECS ALMA survey was essential to identify these sources, which would have been challenging with the VLA data alone. At the same time, the longer-wavelength measurements carried out with the VLA are key to extracting the most reliable constraints on the total gas masses and the scales of any low-excitation gas reservoirs. In the near-term future, ALMA

[27] Quoted uncertainties are one standard deviation for the mean and the median absolute deviation for the median, and exclude absolute flux calibration uncertainties between the VLA and ALMA observations.

[28] The galaxies 9mm.2 and 4 in our sample also contain AGN (Luo et al. 2017; Boogaard et al. 2019).

[29] We also caution that CO line ratios at high redshift are impacted by the warmer cosmic microwave background (CMB), which could increase r_{71} in the presence of low excitation, low brightness temperature gas (e.g., da Cunha et al. 2013).

[30] The formal 1σ range is $\log(\rho(\mathrm{H_2})/M_\odot\,\mathrm{Mpc^{-3}}) = 7.20$–$7.66$.

[31] The formal 1σ range is $\log(\rho(\mathrm{H_2})/M_\odot\,\mathrm{Mpc^{-3}}) = 7.20$–$7.63$.

[32] Given the focus of this work, we here restrict the comparison to results from blank-field CO surveys, and defer comparisons to results from other methods (e.g., Scoville et al. 2017; Liu et al. 2019; Lenkić et al. 2020) to a future publication (R. Decarli et al. 2020, in preparation), but we note that the results from these studies are broadly consistent with those presented here.

[33] These findings assume that the α_{CO} conversion factor for the galaxy populations dominating the signal does not change significantly with redshift, which is consistent with our current constraints.

[34] Since ∼48% of the allocated time for the program remained unobserved from the present effort, three of the detections currently remain tentative.

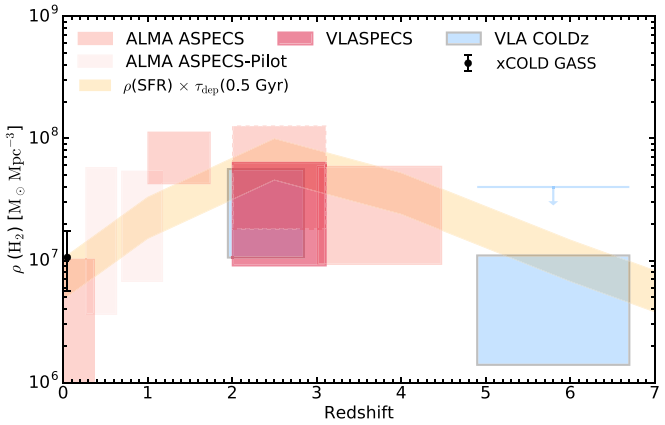

Figure 3. Constraints on the comoving cold gas mass density evolution with redshift from the ASPECS (HUDF; salmon/light red boxes; Decarli et al. 2016, 2019) and COLDz surveys (COSMOS and GOODS-North combined; blue; Riechers et al. 2019), and impact of the new VLASPECS measurements on the $z \sim 2$–3 constraints from ASPECS (crimson red; corrected using the median r_{31}). Vertical sizes indicate uncertainties in each bin (2σ for ASPECS; 90% confidence region for COLDz). COLDz measurements are based on CO($J = 1 \rightarrow 0$) at $z = 2.0$–2.8 and CO($J = 2 \rightarrow 1$) at $z = 4.9$–6.7, whereas ASPECS measurements are based on CO($J = 2 \rightarrow 1$) to CO($J = 4 \rightarrow 3$) in the $z > 0.2$ bins (including CO $J = 3 \rightarrow 2$ at $z = 2.0$–3.1), and CO($J = 1 \rightarrow 0$) in the $z \sim 0$ bin. Other ASPECS redshift bins are left unscaled since no new constraints are available, but at least the $z = 0.3$–0.6, 0.7–1.2, and 3.0–4.5 bins may also require a significant revision. The measurement at $z = 0$ from the xCOLD GASS CO($J = 1 \rightarrow 0$) survey (updated from Saintonge et al. 2017) is shown for comparison. For reference, we also show the total star formation rate density multiplied by an equivalent gas depletion timescale of 0.5 Gyr (Bouwens et al. 2016).

will be able to make similar measurements at $z = 1.2$–2.3 with the addition of Band 1. Our findings suggest that future facilities like the Next Generation Very Large Array (ngVLA; see, e.g., Bolatto et al. 2017) will only achieve their full survey potential when including capabilities at both 9 and 3 mm, as is envisioned in the current baseline plan.

We thank the anonymous referee for a thorough and constructive report. D.R. acknowledges support from the National Science Foundation under grant numbers AST-1614213 and AST-1910107. D.R. also acknowledges support from the Alexander von Humboldt Foundation through a Humboldt Research Fellowship for Experienced Researchers. F.W. acknowledges support from the ERC Advanced grant "Cosmic Gas." I.R.S. acknowledges support from STFC (ST/P000541/1). T.D-.S. acknowledges support from the CASSACA and CONICYT fund CAS-CONICYT Call 2018. J.H. acknowledges support of the VIDI research program with project number 639.042.611, which is (partly) financed by the Netherlands Organization for Scientific Research (NWO). H.I. acknowledges support from JSPS KAKENHI grant No. JP19K23462. M.K. acknowledges support from the International Max Planck Research School for Astronomy and Cosmic Physics at Heidelberg University (IMPRS-HD). Este trabajo contó con el apoyo de CONICYT + PCI + INSTITUTO MAX PLANCK DE ASTRONOMIA MPG190030. The National Radio Astronomy Observatory is a facility of the National Science Foundation operated under cooperative agreement by Associated Universities, Inc. ALMA is a partnership of ESO (representing its member states), NSF (USA) and NINS (Japan), together with NRC (Canada), NSC and ASIAA (Taiwan), and KASI (Republic of Korea), in cooperation with the Republic of Chile. The Joint ALMA Observatory is operated by ESO, AUI/NRAO and NAOJ.

Facilities: VLA data: 19B-131, ALMA data: 2016.1.00324.L.

Appendix
Upper Limit Spectrum for 9mm.7

The upper limit spectrum for 9mm.7 is shown in Figure A1. The source is in a part of the mosaic with low primary beam response (see Table 1), such that the VLA data are only moderately constraining.

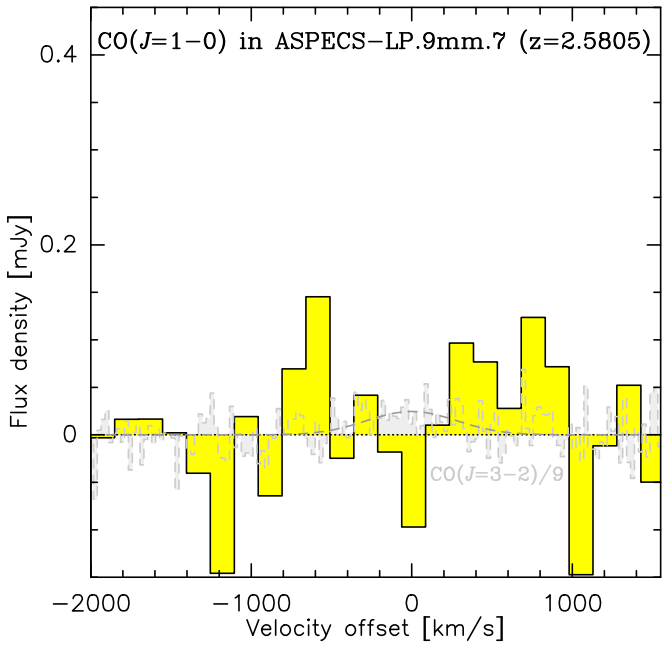

Figure A1. VLA upper limit CO($J = 1 \rightarrow 0$) spectrum of 9mm.7 at a resolution of 125 km s^{-1} (16 MHz), using the same style as in Figure 1.

ORCID iDs

Dominik A. Riechers https://orcid.org/0000-0001-9585-1462
Leindert A. Boogaard https://orcid.org/0000-0002-3952-8588
Roberto Decarli https://orcid.org/0000-0002-2662-8803
Jorge González-López https://orcid.org/0000-0003-3926-1411
Ian Smail https://orcid.org/0000-0003-3037-257X
Fabian Walter https://orcid.org/0000-0003-4793-7880
Manuel Aravena https://orcid.org/0000-0002-6290-3198
Christopher L. Carilli https://orcid.org/0000-0001-6647-3861
Paulo C. Cortes https://orcid.org/0000-0002-3583-780X
Tanio Díaz-Santos https://orcid.org/0000-0003-0699-6083
Jacqueline A. Hodge https://orcid.org/0000-0001-6586-8845
Hanae Inami https://orcid.org/0000-0003-4268-0393
Rob J. Ivison https://orcid.org/0000-0001-5118-1313
Melanie Kaasinen https://orcid.org/0000-0002-1173-2579
Axel Weiß https://orcid.org/0000-0003-4678-3939
Paul van der Werf https://orcid.org/0000-0001-5434-5942

References

Aravena, M., Decarli, R., Gónzalez-López, J., et al. 2019, ApJ, 882, 136
Bennett, C. L., Larson, D., Weiland, J. L., & Hinshaw, G. 2014, ApJ, 794, 135
Bolatto, A. D., Chatterjee, S., Casey, C. M., et al. 2017, arXiv:1711.09960
Bolatto, A. D., Warren, S. R., Leroy, A. K., et al. 2015, ApJ, 809, 175
Bolatto, A. D., Wolfire, M., & Leroy, A. K. 2013, ARA&A, 51, 207
Boogaard, L. A., Decarli, R., González-López, J., et al. 2019, ApJ, 882, 140
Bothwell, M. S., Smail, I., Chapman, S. C., et al. 2013, MNRAS, 429, 3047
Bouwens, R. J., Aravena, M., Decarli, R., et al. 2016, ApJ, 833, 72
Bussmann, R. S., Riechers, D., Fialkov, A., et al. 2015, ApJ, 812, 43
Carilli, C. L., & Walter, F. 2013, ARA&A, 51, 105
Combes, F. 2018, A&ARv, 26, 5
da Cunha, E., Groves, B., Walter, F., et al. 2013, ApJ, 766, 13
Daddi, E., Bournaud, F., Walter, F., et al. 2010, ApJ, 713, 686
Daddi, E., Dannerbauer, H., Liu, D., et al. 2015, A&A, 577, A46
Danielson, A. L. R., Swinbank, A. M., Smail, I., et al. 2011, MNRAS, 410, 1687
Dannerbauer, H., Harrington, K., Díaz-Sánchez, A., et al. 2019, AJ, 158, 34
Decarli, R., Walter, F., Aravena, M., et al. 2016, ApJ, 833, 69
Decarli, R., Walter, F., Carilli, C., et al. 2014, ApJ, 782, 78
Decarli, R., Walter, F., Gónzalez-López, J., et al. 2019, ApJ, 882, 138
Frayer, D. T., Maddalena, R. J., Ivison, R. J., et al. 2018, ApJ, 860, 87
Fu, H., Cooray, A., Feruglio, C., et al. 2013, Natur, 498, 338
Genzel, R., Tacconi, L. J., Lutz, D., et al. 2015, ApJ, 800, 20
Gómez-Guijarro, C., Riechers, D. A., Pavesi, R., et al. 2019, ApJ, 872, 117
González-López, J., Decarli, R., Pavesi, R., et al. 2019, ApJ, 882, 139
Harrington, K. C., Vishwas, A., Weiß, A., et al. 2019, MNRAS, 488, 1489
Illingworth, G. D., Magee, D., Oesch, P. A., et al. 2013, ApJS, 209, 6
Ivison, R. J., Papadopoulos, P. P., Smail, I., et al. 2011, MNRAS, 412, 1913
Kaasinen, M., Scoville, N., Walter, F., et al. 2019, ApJ, 880, 15
Lamperti, I., Saintonge, A., Koss, M., et al. 2020, ApJ, 889, 103
Lenkić, L., Bolatto, A. D., Förster Schreiber, N. M., et al. 2020, AJ, 159, 190
Leung, T. K. D., Riechers, D. A., Baker, A. J., et al. 2019, ApJ, 871, 85
Liu, D., Schinnerer, E., Groves, B., et al. 2019, ApJ, 887, 235
Lu, N., Zhao, Y., Díaz-Santos, T., et al. 2017, ApJS, 230, 1
Luo, B., Brandt, W. N., Xue, Y. Q., et al. 2017, ApJS, 228, 2
Madau, P., & Dickinson, M. 2014, ARA&A, 52, 415
Nayyeri, H., Cooray, A., Jullo, E., et al. 2017, ApJ, 844, 82
Papadopoulos, P. P., van der Werf, P. P., Xilouris, E. M., et al. 2012, MNRAS, 426, 2601
Pavesi, R., Sharon, C. E., Riechers, D. A., et al. 2018, ApJ, 864, 49
Perley, R. A., & Butler, B. J. 2017, ApJS, 230, 7
Popping, G., Pillepich, A., Somerville, R. S., et al. 2019, ApJ, 882, 137
Riechers, D. A., Bradford, C. M., Clements, D. L., et al. 2013, Natur, 496, 329
Riechers, D. A., Carilli, C. L., Walter, F., & Momjian, E. 2010, ApJL, 724, L153
Riechers, D. A., Carilli, L. C., Walter, F., et al. 2011a, ApJL, 733, L11
Riechers, D. A., Cooray, A., Omont, A., et al. 2011b, ApJL, 733, L12
Riechers, D. A., Hodge, J., Walter, F., Carilli, C. L., & Bertoldi, F. 2011c, ApJL, 739, L31
Riechers, D. A., Pavesi, R., Sharon, C. E., et al. 2019, ApJ, 872, 7
Rosenberg, M. J. F., van der Werf, P. P., Aalto, S., et al. 2015, ApJ, 801, 72
Saintonge, A., Catinella, B., Tacconi, L. J., et al. 2017, ApJS, 233, 22
Scoville, N., Lee, N., Vanden Bout, P., et al. 2017, ApJ, 837, 150
Sharon, C. E., Baker, A. J., Harris, A. I., et al. 2015, ApJ, 798, 133
Sharon, C. E., Baker, A. J., Harris, A. I., & Thomson, A. P. 2013, ApJ, 765, 6
Sharon, C. E., Riechers, D. A., Hodge, J., et al. 2016, ApJ, 827, 18
Sharon, C. E., Tagore, A. S., Baker, A. J., et al. 2019, ApJ, 879, 52
Solomon, P. M., & Vanden Bout, P. A. 2005, ARA&A, 43, 677
Tacconi, L. J., Genzel, R., Saintonge, A., et al. 2018, ApJ, 853, 179
Tacconi, L. J., Neri, R., Genzel, R., et al. 2013, ApJ, 768, 74
Thomson, A. P., Ivison, R. J., Smail, I., et al. 2012, MNRAS, 425, 2203
van der Werf, P. P., Isaak, K. G., Meijerink, R., et al. 2010, A&A, 518, L42
Walter, F., Decarli, R., Aravena, M., et al. 2016, ApJ, 833, 67
Walter, F., Decarli, R., Sargent, M., et al. 2014, ApJ, 782, 79
Yao, L., Seaquist, E. R., Kuno, N., & Dunne, L. 2003, ApJ, 588, 771